CONDENSED MATTER PHYSICS

Giant enhancement of exciton diffusivity in two-dimensional semiconductors

Yiling Yu[1], Yifei Yu[1], Guoqing Li[1], Alexander A. Puretzky[2], David B. Geohegan[2], Linyou Cao[1,3,4]*

Two-dimensional (2D) semiconductors bear great promise for application in optoelectronic devices, but the low diffusivity of excitons stands as a notable challenge for device development. Here, we demonstrate that the diffusivity of excitons in monolayer MoS_2 can be improved from 1.5 ± 0.5 to 22.5 ± 2.5 square centimeters per second with the presence of trapped charges. This is manifested by a spatial expansion of photoluminescence when the incident power reaches a threshold value to enable the onset of exciton Mott transition. The trapped charges are estimated to be in a scale of 10^{10} per square centimeter and do not affect the emission features and recombination dynamics of the excitons. The result indicates that trapped charges provide an attractive strategy to screen exciton scattering with phonons and impurities/defects. Pointing towards a new pathway to control exciton transport and many-body interactions in 2D semiconductors.

INTRODUCTION

The transport of charge carriers such as electrons, holes, and excitons consists of the foundation of semiconductor electronic and photonic devices. Therefore, improving the transport of charge carriers in semiconductors is of paramount importance for device development. This is particularly compelling for atomically thin two-dimensional (2D) semiconductors such as MoS_2, WS_2, $MoSe_2$, and WSe_2. These materials provide an attractive platform for the development of next-generation electronic and photonic devices (*1*, *2*). For instance, they present a remarkable exciton system, as manifested by exotic excitonic properties, including electrically tunable optical response (*3*, *4*), exciton phase transition and condensation (*5*, *6*), strong valley-spin coupling (*7*, *8*), room-temperature exciton transistors (*9*), and quantum emission (*10*). However, the atomically thin dimension tends to give rise to inefficient exciton transport, such as low exciton diffusivity, and this represents a significant challenge for the development of novel optoelectronic devices by leveraging on the unique excitonic properties of 2D semiconductors.

Fundamentally, the diffusivity of excitons is dictated by the scattering of excitons with scattering sources including acoustic phonons (via piezoelectric interaction and deformation potential), optical phonons, impurities/defects, and surface roughness (*11*–*13*). Previous studies have extensively demonstrated that the diffusivity of excitons in 2D semiconductors can be improved by reducing the scattering of excitons with substrate-borne scattering sources, for instance, using 2D materials with atomically smooth surfaces such as hexagonal boron nitride as substrates (*12*–*15*). In contrast, the studies to mitigate the exciton scattering with the intrinsic scattering sources in semiconductor materials remained much more limited (*16*). Here, we demonstrate a giant improvement in the diffusivity of excitons at monolayer MoS_2 by one order of magnitude due to the screening of exciton scattering with intrinsic scattering sources. To eliminate the effect of substrates, we performed this study using suspended monolayer MoS_2. The improvement of exciton diffusivity is realized with the presence of trapped charges. This is evidenced by a substantial spatial expansion of photoluminescence (PL) when the incident laser power is comparable to or higher than the threshold power, enabling the onset of exciton Mott transition (EMT). We also demonstrate that the emission features and dynamics of the excitons are preserved with the presence of the trapped charges. The results indicate that trapped charges can screen the scattering of excitons with phonons and impurities/defects. We also roughly estimate that the density of the trapped charges is in scale of 10^{10} cm^{-2}.

RESULTS

Spatial expansion of PL at the onset of EMT

We examine the PL of suspended single-crystalline monolayer MoS_2 as a function of incident laser power. The flakes were grown on SiO_2/Si substrates using a well-established chemical vapor deposition process (*17*) and then transferred to quartz substrates prepatterned with micrometer-scale holes for PL measurement in an Ar environment (see fig. S1 for optical image of the suspended monolayers) (*18*). Figure 1 (A and B) shows typical 2D PL spatial images and 1D PL spatial profiles collected from the monolayer under the incidence of a focused 532-nm laser with different powers. Significantly, whereas the size of the focused laser spot was kept unchanged during the measurement (the gray curve in Fig. 1B), the luminescence area shows a threshold-like expansion at the incident power around 8.0 kW/cm^2. The luminescence area does not change much with variation of the incident power when the power is way lower than 8.0 kW/cm^2, but it substantially expands when the power is increased to be close to 8.0 kW/cm^2 or higher (Fig. 1, A to C). This threshold-like spatial expansion of PL is very reproducible and was observed for every sample studied (more results can be found in fig. S2). Similar threshold-like spatial expansion of PL was also observed at the monolayer MoS_2 supported on substrates, although the threshold power required to enable the expansion is much higher (~30 kW/cm^2; see fig. S3).

The incident power can enable a temperature increase and also induce possible defect generation at the monolayer. However, our experimental results indicate that neither the temperature increase nor the generation of defects is responsible for the observed spatial

[1]Department of Materials Science and Engineering, North Carolina State University, Raleigh, NC 27695, USA. [2]Center for Nanophase Materials Sciences, Oak Ridge National Laboratory, Oak Ridge, TN 37831, USA. [3]Department of Physics, North Carolina State University, Raleigh, NC 27695, USA. [4]Department of Electrical and Computer Engineering, North Carolina State University, Raleigh, NC 27695, USA.
*Corresponding author. Email: linyoucao@gmail.com

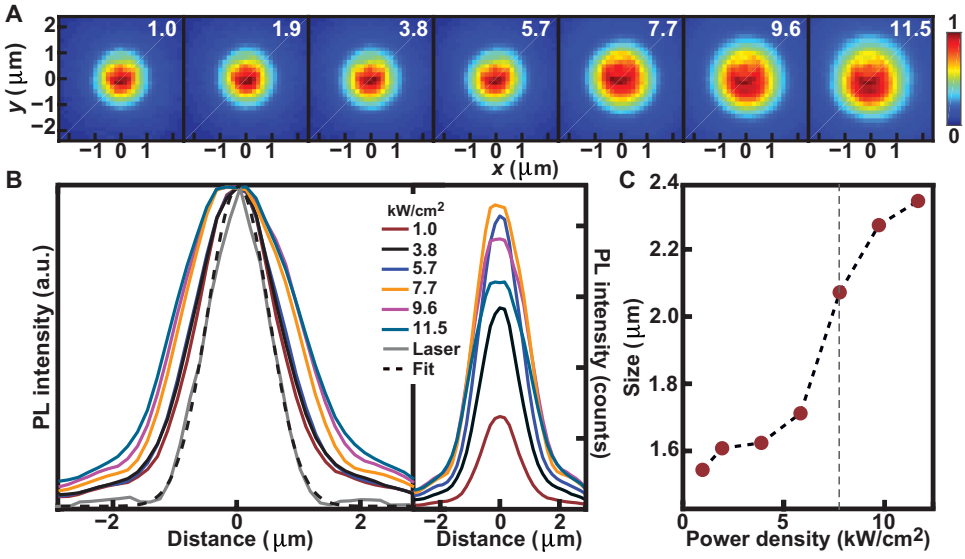

Fig. 1. Threshold-like spatial luminescence expansion of monolayer MoS_2. (**A**) PL images collected from a typical suspended monolayer MoS_2 under the incidence of different laser powers, as indicated by the white numbers (kilowatts per square centimeter in units). The time interval between each measurement is around 1 min. (**B**) Normalized spatial profiles of PL intensity across the monolayer MoS_2. The spatial profiles of the focused laser beam (gray solid curve) and related fitting (dashed black curve) are also plotted. The right panel shows the as-measured spatial profiles of PL intensity without normalization. a.u., arbitrary units. (**C**) The size of the luminescence area (full width at half magnitude of the spatial profile) as a function of the incident power. The vertical dashed lines indicate the sudden spatial expansion. Error bars are not given in (C) for visual convenience because the error bars are comparable to the size of the dots.

expansion of PL. First, we placed the suspended monolayer in a Linkam heating/cooling stage and monitored the PL of the monolayer as a function of well-controlled temperature increase. The luminescence area tends to slightly shrink with the temperature increasing (Fig. 2, A and B), which indicates that the increase in temperature is not responsible for the observed PL expansion. In addition, the spatial expansion of PL was found to be reversible, as the expanded luminescence area shrinks back to the original dimension upon mild annealing at 100°C or after being held for several hours at room temperature, as will be discussed later. This reversibility indicates that the luminescence expansion is not due to defect generation, where such effect would be long lived. This matches our intuitive expectation since the threshold power (~8.0 kW/cm^2) is not high enough to induce defect generation. It is also supported by the similar Raman spectra from the monolayer before and after the PL measurement (fig. S4), which confirms no major damage in the composition/structure of the monolayer during the measurement.

A possible mechanism that could enable a spatial expansion of PL with the increase in incident power is the presence of strong nonlinear exciton recombination, such as exciton-exciton annihilation (EEA) (*19*). However, we can exclude the nonlinear exciton recombination as the mechanism for the observed PL expansion as well. We schematically illustrate the effect of EEA on the spatial profile of PL in Fig. 2C, in which the exciton diffusion is ignored for simplicity. The PL spatial profile would be identical to the incident laser spatial profile under linear exciton recombination, but broader than the incident laser profile with the presence of strong EEA, because EEA enables lower PL efficiencies at higher incident powers. EEA increases with exciton density faster than linear exciton recombination. Therefore, the increase in incident power could enable the exciton recombination to evolve from being linear to EEA dominated, which would result in a spatial expansion of PL. However, the spatial expansion

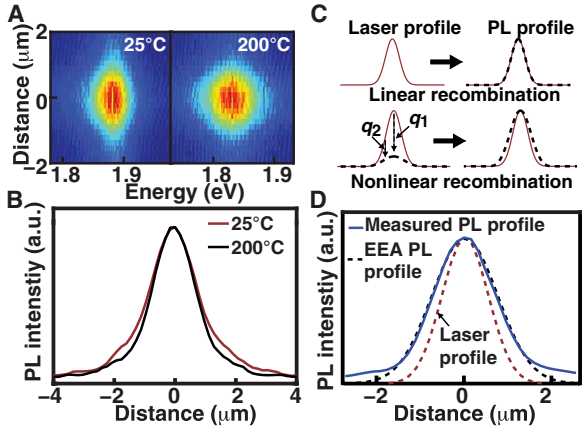

Fig. 2. Effect of temperature increase and nonlinear exciton recombination on PL profile. (**A**) Typical spectral-spatial PL images collected from monolayer MoS_2 at different environment temperatures (25° and 200°C) under the incidence of 1.0 kW/cm^2, in which the vertical axis is the distance and the horizontal axis is the energy. The spectra at 200°C are broader than those 25°C, but the spatial distribution at 200°C is slightly smaller than that at 25°C. (**B**) Normalized spatial profiles of PL intensity at 25° and 200°C that are extracted from (A). (**C**) Schematically illustrates the PL spatial profile under linear and nonlinear exciton recombination. q_1 and q_2 indicate space-variant PL efficiencies. (**D**) Overlap of the measured PL profile (at 1.0 kW/cm^2) with the PL profile expected for EEA-dominated exciton recombination and negligible diffusion, which is square root of the laser profile, as $\exp(-r^2/w^2)$. The Gaussian laser profile $\exp(-2r^2/w^2)$ is also plotted as reference.

of PL enabled by the effect of EEA is continuous with the increase in incident power (*19*), different from the threshold-like expansion at ~8.0 kW/cm^2 observed in our experiments. In addition, our analysis indicates that EEA dominates the exciton recombination in monolayer

MoS_2 even at the lowest incident power (1.0 kW/cm^2) used in the experiment (see section S1 for detailed analysis). We find that the PL spatial profiles measured at low incident powers match the PL spatial profile predicted for EEA-dominated recombination (Fig. 2D) (see section S1 for detailed analysis), which supports the dominance of EEA in the exciton recombination at even the lowest incident power. Therefore, further increasing the incident power cannot induce the change of exciton recombination from being linear to EEA dominated. The presence of strong EEA in monolayer MoS_2 cannot cause the observed spatial expansion of PL.

Instead, we can correlate the threshold-like spatial expansion of PL to the onset of EMT, at which excitons are ionized into a stable plasma of free electrons and holes [referred as electron-hole plasma (EHP)]. This is evidenced by the changes in the PL spectral features accompanying the spatial expansion, which matches the characteristic PL spectral features associated with the onset of EMT (*5*, *20*). Figure 3A shows the PL spectra collected from the monolayer MoS_2 at different laser powers. The spectral features of the PL, including spectral width (Fig. 3B), peak position (Fig. 3C), and intensity (Fig. 3D) are plotted as a function of the incident power. Similar to the spatial expansion, the spectral features also show threshold-like changes at the incident power of around 8.0 kW/cm^2. More specifically, the broadening and red shift at the incident power of <8.0 kW/cm^2 can be ascribed to the temperature increase induced by the photothermal effect of the incident laser (dashed lines in Fig. 3, B and C, and see temperature analysis in section S2), but the photothermal effect cannot account for the broadening and red shift at the incident power of >8.0 kW/cm^2. In addition, the PL intensity increases with the incident power when the power is <8.0 kW/cm^2, but it turns to be pretty much power independent at the power of >8.0 kW/cm^2 (Fig. 3E). These changes are consistent with the characteristic PL spectral features associated with the onset of EMT, as reported previously (*5*, *20*). Briefly, the broadening increase is due to the emergence of emission from EHP, the smaller red shift is related to the screening effect of the free charges in EHP on both bandgap and exciton binding energy that offsets the thermally induced red shift, and the negligible power dependence of the PL intensity results from the opposite changes in the emission of excitons (decrease) and EHP (increase) with increase in the incident power. Intuitively, excitons consist of pairwise electrons and holes bound by electrostatic forces, and pairwise electrostatic force can be screened with the presence of a high density of charges. EMT can be enabled when the charge density is higher than certain threshold value, which is on the order of 10^{12} cm^2 in monolayer MoS_2, to enable screening length comparable to exciton Bohr radius (*5*, *20*). This is consistent with the threshold-like nature in the observed changes of the PL's spatial and spectral features.

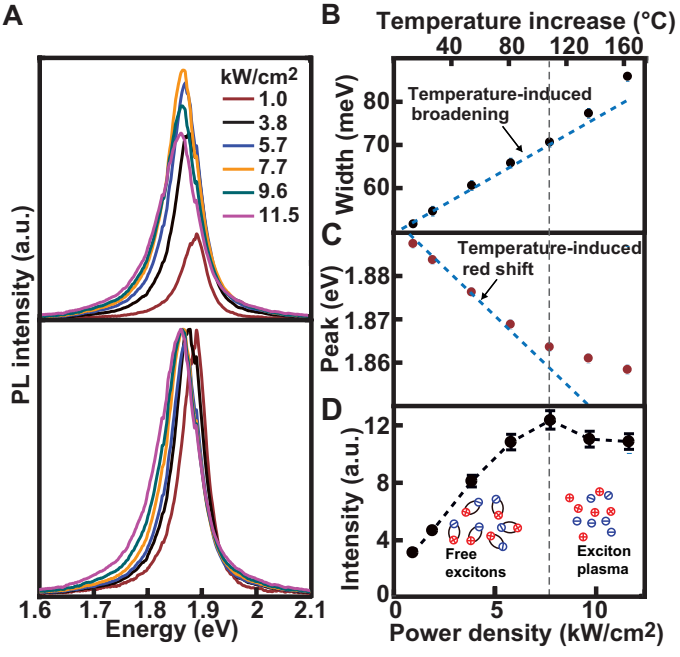

Fig. 3. Threshold-like evolution of PL spectral features with the incident power. (**A**) As-measured (top) and normalized (bottom) PL spectra collected from monolayer MoS_2 under different incident powers. (**B**) The PL's spectral full width at half magnitude, (**C**) the PL's peak position, and (**D**) the PL intensity (black circles) as a function of the incident power. The vertical dashed line in (B) to (D) indicates the threshold power for sudden spectra features change and PL intensity change. The spectral broadening and red shift caused by the laser-induced temperature increase are also plotted in (B) and (C), respectively. The inset in (D) schematically illustrates the ionization of excitons. Error bars are not given in (C) and (D) because the error bars are comparable to the size of the dots.

Role of trapped charges in the spatial expansion of PL

The coincidence of the PL spatial expansion with the onset of EMT strongly suggests that the free charges resulting from exciton ionization play a critical role in the expansion. More specifically, experimental results indicate that the charges trapped in the monolayer enable the spatial expansion. We examined the PL at the same spot of monolayer MoS_2 by alternating the incident power back and forth. As shown in Fig. 4A, we first collected PL with 1.1 kW/cm^2 (first measurement) and then increased the power to 8.0 kW/cm^2 for PL measurement (second measurement). After that, we lowered the power to 1.1 kW/cm^2 and measured the PL again (third measurement). The luminescence area expanded when the incident power was increased from 1.1 to 8.0 kW/cm^2 (Fig. 4, A and B). However, the expanded luminescence area did not shrink when the incident power was lowered back to 1.1 kW/cm^2. Compared to the low-power PL collected at the first measurement, the low-power PL measured at the third measurement shows obviously lower intensity at the center but higher intensity at the peripheral region, as shown in Fig. 4C. We annealed the monolayer at 100°C for 30 min in an Ar environment (which is mild and does not cause any damage to the monolayer), cooled it to room temperature, and then measured the PL with the incident power of 1.1 kW/cm^2 (fourth measurement). The PL recovers to be similar to that of the first measurement, including shrinking of the luminescence area (Fig. 4C) and an increase in the intensity (Fig. 4D). The expanded luminescence area enabled by high-power laser incidence can also shrink back and recover the original dimension by simply keeping the monolayer at room temperature for hours (fig. S5).

These experimental observations indicate that the PL spatial expansion is driven by the charges trapped in the monolayer. Upon the onset of the EMT, excitons are ionized into a stable plasma of free electrons and holes. Some of the resulting charges are trapped in the monolayer, and the trapped charges can persist even after the photoexcitation is turned off. This accounts for the observation that the expanded luminescence area enabled at high photoexcitation does not shrink back immediately after the incident power is lowered. The correlation to trapped charges is also supported by the recovery

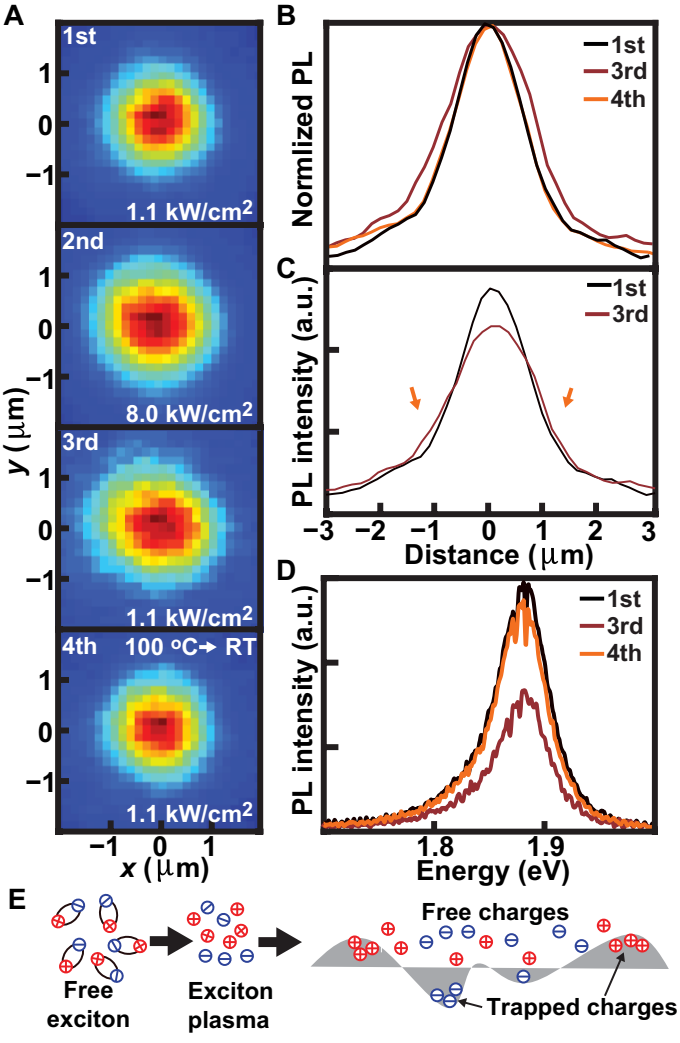

Fig. 4. Effect of trapped charges on the PL spatial expansion. (**A**) PL images collected from the same monolayer with different incident powers in sequence: 1.1 kW/cm^2 (first measurement), 8.0 kW/cm^2 (second measurement), 1.1 kW/cm^2 (third measurement), and 1.1 kW/cm^2 again (fourth measurement) after raising temperature to 100°C then cooling back to room temperature 25°C (RT). The time interval between each of the first three measurements is around 1 min. The heating process takes time of 10 min, and cooling takes 30 min. (**B**) Normalized spatial profiles of PL intensity collected at the different measurements using 1.1 kW/cm^2 (first, third, and fourth measurement). (**C**) Spatial profiles of PL intensity collected at the first and third measurements. The orange arrows point to the peripheral region. (**D**) PL spectra collected at the first, third, and fourth measurements. (**E**) Schematic illustration for free charges and trapped charges resulting from exciton ionization.

of the low-power PL spatial and spectral features after the annealing treatment or holding for hours at room temperatures. It is well known that trapped charges can slowly be released under room temperature, and thermal annealing can facilitate the release.

To get more insight into the effect of trapped charges, we examine the spatial distribution of photogenerated charge carriers. Intuitively, the photogenerated charge carriers simultaneously experience recombination and diffusion. In a steady state, the spatial distribution of the photogenerated charge carriers $n(r)$ in the monolayer under the incidence of a focused Gaussian laser can be written as

$$-n(r)/\tau + k[n(r)]^2 + D\nabla^2 n(r) + \alpha P_0 \exp(-2r^2/w^2) = 0 \quad (1)$$

where τ is the linear recombination time, k is the EEA rate, α is the absorption efficiency of the monolayer for the incident laser, P_0 is the incident power density at the center, w is the radius of the focused laser beam, and D is the diffusion coefficient of excitons. We have confirmed that the absorption efficiency does not change with the incident power (fig. S6). Therefore, the diffusion coefficient D and the exciton recombination (τ and k) are the only parameters that could give rise to the observed threshold-like spatial expansion of PL with increase in the incident power. As we have identified trapped charges to be the major driving force for the spatial expansion, the key issue is to find out how the trapped charges could affect the diffusion (D) and recombination (τ and k) and how the effects could enable the spatial expansion.

We can conclude that the effect of trapped charge on the exciton recombination cannot enable the spatial expansion of the PL based on intuitive analysis of Eq. 1. EEA dominates the exciton recombination in our experiment (see section S1 for detailed analysis). According to Eq. 1, the spatial profile of PL with EEA-dominated recombination would maintain a constant shape as $\exp(-r^2/w^2)$ regardless of the incident power if the diffusivity is low ($D \approx 0$). All the PL spatial profiles measured at low incident powers (<8.0 kW/cm^2) are reasonably close to the profile described by $\exp(-r^2/w^2)$, as shown in Fig. 2D. With low diffusivity ($D \approx 0$) and EEA-dominated recombination, the effect of trapped charges on τ and k would only be able to cause the spatial profile of PL shrinking from the EEA-dominating profile [$\exp(-r^2/w^2)$] to the linear recombination–dominating profile [$\exp(-2r^2/w^2)$]. There is no way that the effect of trapped charges on τ and k can enable expansion of the PL profile.

This conclusion is also supported by the negligible effect of the trapped charges on exciton recombination. We studied the exciton dynamics at suspended MoS_2 monolayers with pump-probe techniques in previous studies (*21*) and found no obvious change in exciton dynamics when repeatedly measuring the same spot with alternating pump fluences back and forth (*21*). A typical result is plotted in Fig. 5A. We first measured the dynamics with a low pumping energy fluence of 1.9 μJ/cm^2 per pulse, then measured it with a high pumping fluence of 12.8 μJ/cm^2 per pulse, and lastly lowered the fluence back to 1.9 μJ/cm^2 per pulse for measurement again (see section S3 for more details). The time interval between each of these measurements was less than 10 min. The low pumping fluence of 1.9 μJ/cm^2 per pulse is designed to generate less charge carriers much less than the incident power of 8.0 kW/cm^2, and the high pumping fluence of 12.8 μJ/cm^2 per pulse is to generate more charge carriers than 8.0 kW/cm^2. There is no observable difference in the dynamics at low pumping fluences before and after the incidence of the high pumping fluence, indicating a negligible effect of trapped charges on the charge dynamics.

The negligible effect of the trapped charges on exciton dynamics is corroborated by the preservation of emission features of the excitons with the presence of the trapped charges, which indicates a weak capability of the trapped charges to facilitate the conversion of neutral excitons to charged excitons. It has been well documented that free charges can combine with neutral excitons to form charged excitons, and charged excitons have different dynamics from neutral excitons (*3*, *4*, *22*). However, trapped charges do not combine with neutral excitons in the same way as free charges do. Figure 5B

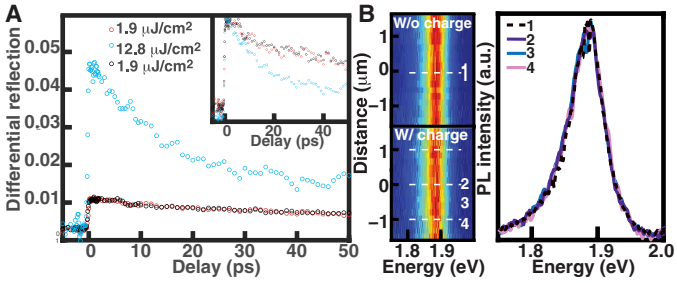

Fig. 5. Effect of trapped charges on exciton recombination. (**A**) Pump-probe measurement results in suspended monolayer MoS_2 under different pumping fluences. The inset is the result after being normalized to the value at 0 s. The measurements were performed with a pumping fluence of 1.9 μJ/cm^2 per pulse (red), 12.8 μJ/cm^2 per pulse (cyan), and 1.9 μJ/cm^2 per pulse (black) in a sequence on the same spot. More experimental details can be found at our previous studies (*21*). The time interval between each of the measurement is around 10 min. (**B**) Normalized spatial-spectral PL images collected from monolayer MoS_2 with low incident powers (1.1 kW/cm^2) before (without trapped charges) and after (with trapped charges) the incidence of high photoexcitation (8.0 kW/cm^2). They are collected at the first and third measurements in Fig. 4. The spectra at each location are normalized with respect to its own peak intensity, and the unnormalized results are plotted in fig. S7. The right panel shows typical spectra extracted from the spatial-spectra images, as indicated by dashed white lines.

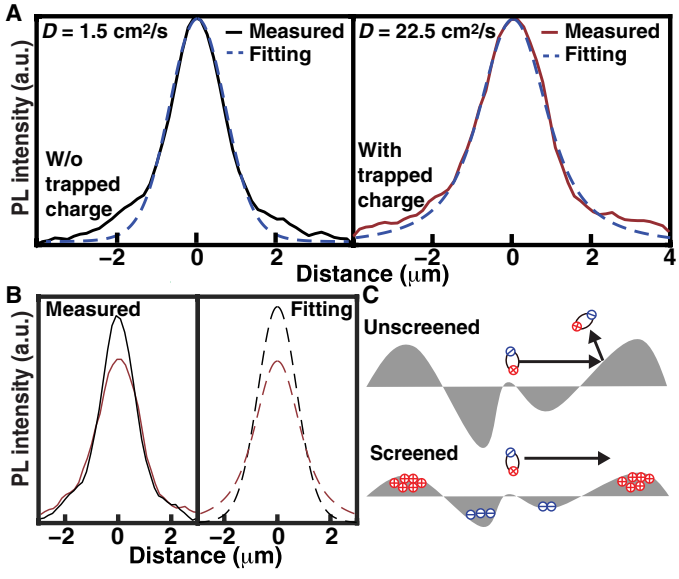

Fig. 6. Enhancement of exciton diffusion coefficient. (**A**) Fitting and measured spatial profiles of PL intensity collected with low incident powers (1.0 kW/cm^2) before (without trapped charges) and after (with trapped charges) the incidence of high photoexcitation (8.0 kW/cm^2). The experimental results were collected at the first and third measurements in Fig. 4. The fitting results for the diffusion coefficient are given, as shown. (**B**) Comparison illustrating the consistence of the fitted PL intensity with the experimental result. (**C**) Schematic illustration for the screening of trapped charges for exciton scattering.

shows the normalized 2D spatial-spectra PL images (the spectra at each location are normalized with respect to its own peak intensity, and the unnormalized results are plotted in fig. S7) collected from a monolayer with and without the presence of trapped charges (collected at the first and third measurements in Fig. 4). We find no difference in the PL spectra peak positions and spectral widths with or without trapped charges, both featuring a peak at ~1.89 eV and with a width of ~60 meV that is characteristic emission of the neutral *A* exciton of monolayer MoS_2. According to previous studies (*3*, *4*, *22*–*24*), we would expect a red shift and broadening in PL emission if the trapped charges induce the conversion of neutral excitons to charged excitons. The spectral-spatial image also shows no difference in the PL spectral feature across the luminescence area, and this indicates that trions, if any, diffuse together with excitons.

Enhancement of exciton diffusion with the presence of trapped charges

On basis of all the above-mentioned discussion, we can conclude that the only viable mechanism to enable the observed PL spatial expansion is enhancement of the diffusivity *D* by trapped charges. We can quantitatively evaluate the increase in *D* enabled by the trapped charges through fitting the measured spatial profile of PL intensity using Eq. 1. All the parameters except *D* in Eq. 1 can be obtained from experimental measurement. α is found to be 0.065 based on the analysis with the refractive index of monolayer MoS_2 (fig. S8) (*25*). *w* is measured to be 1.10 μm (Fig. 1B). τ and *k* can be found to be around 1.0 ns and 0.04 cm^2/s, respectively, from our ultrafast spectroscopic and power-dependent PL measurement, which is consistent with our previous result and the result in references (*19*, *21*, *26*–*28*). Typical fitting result for the low-power PL with and without trapped charges is plotted in Fig. 6 (A and B). The fitting reasonably reproduces the major features associated with the spatial expansion. These include a broader spatial profile of PL intensity (Fig. 6A) and an intensity decrease by around 25 to 30% at the luminescence center (Fig. 6B). The fitting indicates that the diffusion coefficient of excitons is ~1.5 ± 0.5 cm^2/s with no trapped charge, consistent with the results of many previous reports (*13*, *14*, *27*, *29*, *30*). The fitting also indicates that the diffusion coefficient sharply increases by more than one order of magnitude to 22.5 ± 2.5 cm^2/s with the presence of trapped charges.

Fundamentally, the diffusivity of excitons is governed by the scattering of excitons with scattering sources such as acoustic phonons (via piezoelectric interaction and deformation potential), optical phonons, impurities/defects, and surface roughness, which changes the excitons' momentum and energy (*11*–*13*, *31*). The improvement of diffusivity with the presence of trapped charges indicates that the scattering of excitons can be substantially screened by trapped charges. As illustrated in Fig. 6C, the presence of trapped charges could screen the scattering potential to make the transport of excitons more smoothly. This conclusion is supported by similar observations in the literature for substantial enhancements in the diffusivity of charge carriers in the presence of a large density of charge carriers (*32*–*37*). In addition, a recent study explicitly demonstrated that exciton-phonon scattering in 2D semiconductors may be suppressed with the injection of charges (*16*).

We can roughly estimate the density of the trapped charges. The density of free charges in monolayer MoS_2 upon the onset of EMT is around 1.0×10^{12} cm^{-2} (*20*). We also estimate from experimental results that the energy barrier ΔE for charge trapping in monolayer MoS_2 is in the range of 160 to 190 meV (see analysis of defect energy level in section S4). The average temperature *T* of the monolayer under the incidence of 8.0 kW/cm^2 is around 410 K, as shown in Fig. 3C. Following the well-established equation for charge trapping

efficiency, $\exp(-\Delta E/k_BT)$, where k_B is the Boltzmann constant, we can estimate that the trapping efficiency is around 1% and the density of the trapped charge is ~10^{10} cm^{-2}. The dominant defects in single-crystalline monolayer MoS_2 are sulfur vacancies due to the nonstoichiometric nature of the materials (*38*), and these defects might serve as a trapping center for charges.

DISCUSSION

In conclusion, we have demonstrated a giant improvement in the diffusivity of excitons at monolayer MoS_2 from ~1.5 ± 0.5 to ~22.5 ± 2.5 cm^2/s with the presence of trapped charges and estimated that the density of the trapped charges is in scale of 10^{10} cm^{-2}. The result indicates that the trapped charges can effectively screen the scattering of excitons with scattering sources such as impurities/defects and phonons. We also demonstrate that unlike free charges, these trapped charges do not combine with excitons to form charged excitons nor do they change the recombination dynamics of the excitons. This indicates that the presence of trapped charges can preserve the dynamics of excitons, which is very useful from the standpoint of applications. Our studies are mainly focused on suspended MoS_2 monolayers, but the conclusion holds for substrate-supported MoS_2 (fig. S3) and other 2D semiconductors such as WS_2 (fig. S9), $MoSe_2$, and WSe_2. In this work, the trapped charges are injected by photoexcitation, but the giant improvement in exciton diffusivity may hold true for the trapped charges injected by other ways, for instance, electrical injection. This study opens up a new avenue to control exciton transport for the development of high-performance excitonic devices, such as exciton transistors, solar energy conversion devices, and photodetectors. The result also points out a new versatile way to control other many body interactions in 2D semiconductors, for instance, improving the mobility of electrons and holes by suppressing electron-phonon scattering via trapped charges.

MATERIALS AND METHODS

Synthesis and transfer and monolayer MoS_2

The monolayer was grown on SiO_2/Si substrates using a well-established chemical vapor deposition process (*26*) and then was transferred onto the quartz substrates with prepatterned blind holes with a depth of around 2 μm using a surface energy–assisted transfer approach (*27*). The holes were fabricated using standard photolithography and dry etching processes. In a typical transfer process, 9 g of polystyrene [PS; molecular weight, 280 kg/mol] was dissolved in 100 ml of toluene. The PS solution was spin-coated (3000 rpm for 60 s) on the as-grown monolayer, followed by baking at 85°C for 1 hour. A water droplet was then dropped to assist the lift off of the PS-monolayer assembly. The polymer-monolayer assembly was transferred to the quartz substrate and baked at 150°C for 30 min. The transfer sample was rinsed with toluene to remove PS and annealed at 80°C for 30 min.

Optical characterization

PL measurements were performed at a home-built setup consisted of a 532-nm laser (Coherent Verdi), a spectrometer (Acton SP2300), and a charge-coupled device camera (PIXIS100). The incident laser was focused onto the monolayer through a long-distance 50× objective, and PL was collected through the same objective. The spatial PL images were collected using zeroth-order grating of the spectrometer, and the spatial-spectral PL image was collected using first-order grating of the spectrometer. All the PL and reflection measurements were conducted with the monolayers located in a Linkam heating/cooling stage with Ar gas flowing. Unless explicitly specified, all the PL measurements were conducted at room temperature (298 K).

SUPPLEMENTARY MATERIALS

Supplementary material for this article is available at http://advances.sciencemag.org/cgi/content/full/6/51/eabb4823/DC1

REFERENCE AND NOTES

1. M.-Y. Li, S.-K. Su, H.-S. P. Wong, L.-J. Li, How 2D semiconductors could extend Moore's law. *Nature* **567**, 169–170 (2019).
2. T. Mueller, E. Malic, Exciton physics and device application of two-dimensional transition metal dichalcogenide semiconductors. *npj 2d Mater. Appl.* **2**, 29 (2018).
3. Y. Yu, Y. Yu, L. Huang, H. Peng, L. Xiong, L. Cao, Giant gating tunability of optical refractive index in transition metal dichalcogenide monolayers. *Nano Lett.* **17**, 3613–3618 (2017).
4. K. F. Mak, K. L. He, C. Lee, G. H. Lee, J. Hone, T. F. Heinz, J. Shan, Tightly bound trions in monolayer MoS_2. *Nat. Mater.* **12**, 207–211 (2013).
5. Y. Yu, A. W. Bataller, R. Younts, Y. Yu, G. Li, A. A. Puretzky, D. B. Geohegan, K. Gundogdu, L. Cao, Room-temperature electron–hole liquid in monolayer MoS_2. *ACS Nano* **13**, 10351–10358 (2019).
6. Z. Wang, D. A. Rhodes, K. Watanabe, T. Taniguchi, J. C. Hone, J. Shan, K. F. Mak, Evidence of high-temperature exciton condensation in two-dimensional atomic double layers. *Nature* **574**, 76–80 (2019).
7. J. R. Schaibley, H. Yu, G. Clark, P. Rivera, J. S. Ross, K. L. Seyler, W. Yao, X. Xu, Valleytronics in 2D materials. *Nat. Rev. Mater.* **1**, 16055 (2016).
8. X. Xu, W. Yao, D. Xiao, T. F. Heinz, Spin and pseudospins in layered transition metal dichalcogenides. *Nat. Phys.* **10**, 343–350 (2014).
9. D. Unuchek, A. Ciarrocchi, A. Avsar, K. Watanabe, T. Taniguchi, A. Kis, Room-temperature electrical control of exciton flux in a van der Waals heterostructure. *Nature* **560**, 340–344 (2018).
10. Y.-M. He, G. Clark, J. R. Schaibley, Y. He, M.-C. Chen, Y.-J. Wei, X. Ding, Q. Zhang, W. Yao, X. Xu, C.-Y. Lu, J.-W. Pan, Single quantum emitters in monolayer semiconductors. *Nat. Nanotechnol.* **10**, 497–502 (2015).
11. K. Kaasbjerg, K. S. Thygesen, A. P. Jauho, Acoustic phonon limited mobility in two-dimensional semiconductors: Deformation potential and piezoelectric scattering in monolayer MoS_2 from first principles. *Phys. Rev. B* **87**, 235312 (2013).
12. N. Ma, D. Jena, Charge scattering and mobility in atomically thin semiconductors. *Phys. Rev. X* **4**, 011043 (2014).
13. A. Raja, L. Waldecker, J. Zipfel, Y. Cho, S. Brem, J. D. Ziegler, M. Kulig, T. Taniguchi, K. Watanabe, E. Malic, T. F. Heinz, T. C. Berkelbach, A. Chernikov, Dielectric disorder in two-dimensional materials. *Nat. Nanotechnol.* **14**, 832–837 (2019).
14. F. Cadiz, C. Robert, E. Courtade, M. Manca, L. Martinelli, T. Taniguchi, K. Watanabe, T. Amand, A. C. H. Rowe, D. Paget, B. Urbaszek, X. Marie, Exciton diffusion in WSe_2 monolayers embedded in a van der Waals heterostructure. *Appl. Phys. Lett.* **112**, 152106 (2018).
15. S. Hao, M. Z. Bellus, D. He, Y. Wang, H. Zhao, Controlling exciton transport in monolayer $MoSe_2$ by dielectric screening. *Nanoscale Horiz.* **5**, 139–143 (2020).
16. B. Miller, J. Lindlau, M. Bommert, A. Neumann, H. Yamaguchi, A. Holleitner, A. Hogele, U. Wurstbauer, Tuning the Fröhlich exciton-phonon scattering in monolayer MoS_2. *Nat. Commun.* **10**, 807 (2019).
17. Y. Yu, S. Hu, L. Su, L. Huang, Y. Liu, Z. Jin, A. A. Purezky, D. B. Geohegan, K. W. Kim, Y. Zhang, L. Cao, Equally efficient interlayer exciton relaxation and improved absorption in epitaxial and nonepitaxial MoS_2/WS_2 heterostructures. *Nano Lett.* **15**, 486–491 (2014).
18. A. Gurarslan, Y. F. Yu, L. Q. Su, Y. L. Yu, F. Suarez, S. Yao, Y. Zhu, M. Ozturk, Y. Zhang, L. Y. Cao, Surface-energy-assisted perfect transfer of centimeter-scale monolayer and few-layer MoS_2 films onto arbitrary substrates. *ACS Nano* **8**, 11522–11528 (2014).
19. M. Kulig, J. Zipfel, P. Nagler, S. Blanter, C. Schuller, T. Korn, N. Paradiso, M. M. Glazov, A. Chernikov, Exciton diffusion and halo effects in monolayer semiconductors. *Phys. Rev. Lett.* **120**, 207401 (2018).
20. Y. Yu, G. Li, L. Cao, Exciton Mott transition in two-dimensional semiconductors. arXiv:2007.11509 [cond-mat.mtrl-sci] (16 September 2020).
21. Y. Yu, Y. Yu, C. Xu, A. Barrette, K. Gundogdu, L. Cao, Fundamental limits of exciton-exciton annihilation for light emission in transition metal dichalcogenide monolayers. *Phys. Rev. B* **93**, 201111 (2016).
22. Y. F. Yu, Y. L. Yu, C. Xu, Y. Q. Cai, L. Q. Su, Y. Zhang, Y. W. Zhang, K. Gundogdu, L. Y. Cao, Engineering substrate interactions for high luminescence efficiency of transition-metal dichalcogenide monolayers. *Adv. Funct. Mater.* **26**, 4733–4739 (2016).

23. Y. Yu, G. Li, L. Huang, A. Barrette, Y.-Q. Cai, Y. Yu, K. Gundogdu, Y.-W. Zhang, L. Cao, Enhancing multifunctionalities of transition-metal dichalcogenide monolayers *via* cation intercalation. *ACS Nano* **11**, 9390–9396 (2017).
24. Y. Lin, X. Ling, L. Yu, S. Huang, A. L. Hsu, Y.-H. Lee, J. Kong, M. S. Dresselhaus, T. Palacios, Dielectric screening of excitons and trions in single-layer MoS_2. *Nano Lett.* **14**, 5569–5576 (2014).
25. Y. Yu, Y. Yu, Y. Cai, W. Li, A. Gurarslan, H. Peelaers, D. E. Aspnes, C. G. V. Walle, N. V. Nguyen, Y.-W. Zhang, L. Cao, Exciton-dominated dielectric function of atomically thin MoS_2 films. *Sci. Rep.* **5**, 16996 (2015).
26. D. Sun, Y. Rao, G. A. Reider, G. Chen, Y. You, L. Brézin, A. R. Harutyunyan, T. F. Heinz, Observation of rapid exjciton–exciton annihilation in monolayer molybdenum disulfide. *Nano Lett.* **14**, 5625–5629 (2014).
27. S. Mouri, Y. Miyauchi, M. Toh, W. J. Zhao, G. Eda, K. Matsuda, Nonlinear photoluminescence in atomically thin layered WSe_2 arising from diffusion-assisted exciton-exciton annihilation. *Phys. Rev. B* **90**, 155449 (2014).
28. L. Yuan, L. Huang, Exciton dynamics and annihilation in WS_2 2D semiconductors. *Nanoscale* **7**, 7402–7408 (2015).
29. L. Yuan, T. Wang, T. Zhu, M. Zhou, L. Huang, Exciton dynamics, transport, and annihilation in atomically thin two-dimensional semiconductors. *J. Phys. Chem. Lett.* **8**, 3371–3379 (2017).
30. T. Zhu, L. Yuan, Y. Zhao, M. Zhou, Y. Wan, J. Mei, L. Huang, Highly mobile charge-transfer excitons in two-dimensional WS_2/tetracene heterostructures. *Sci. Adv.* **4**, eaao3104 (2018).
31. M. Lundstrom, *Fundamentals of Carrier Transport* (Cambridge Univ., 2000).
32. M. M. Perera, M.-W. Lin, H.-J. Chuang, B. P. Chamlagain, C. Wang, X. Tan, M. M.-C. Cheng, D. Tomanek, Z. X. Zhou, Improved carrier mobility in few-layer MoS_2 field-effect transistors with ionic-liquid gating. *ACS Nano* **7**, 4449–4458 (2013).
33. T. L. Atallah, J. Wang, M. Bosch, D. Seo, R. A. Burke, O. Moneer, J. Zhu, M. Theibault, L. E. Brus, J. Hone, X.-Y. Zhu, Electrostatic Screening of charged defects in monolayer MoS_2. *J. Phys. Chem. Lett.* **8**, 2148–2152 (2017).
34. B. W. H. Baugher, H. O. H. Churchill, Y. F. Yang, P. Jarillo-Herrero, Intrinsic electronic transport properties of high-quality monolayer and bilayer MoS_2. *Nano Lett.* **13**, 4212–4216 (2013).
35. L. Chu, H. Schmidt, J. Pu, S. Wang, B. Ozyilmaz, T. Takenobu, G. Eda, Charge transport in ion-gated mono-, bi-, and trilayer MoS_2 field effect transistors. *Sci. Rep.* **4**, 7293 (2014).
36. B. Radisavljevic, A. Kis, Mobility engineering and a metal-insulator transition in monolayer MoS_2. *Nat. Mater.* **12**, 815–820 (2013).
37. K. K. H. Smithe, C. D. English, S. V. Suryavanshi, E. Pop, High-field transport and velocity saturation in synthetic monolayer MoS_2. *Nano Lett.* **18**, 4516–4522 (2018).
38. W. Zhou, X. Zou, S. Najmaei, Z. Liu, Y. Shi, J. Kong, J. Lou, P. M. Ajayan, B. I. Yakobson, J.-C. Idrobo, Intrinsic structural defects in monolayer molybdenum disulfide. *Nano Lett.* **13**, 2615–2622 (2013).

Acknowledgments: We acknowledge the use of the Analytical Instrumentation Facility (AIF) at North Carolina State University, which is supported by the State of North Carolina and the NSF. Part of the Raman and PL measurements was conducted at the Center for Nanophase Materials Sciences, which is a DOE Office of Science User Facility. We also acknowledge C. Xu and K. Gundogdu for help with the pump-probe measurement. **Funding:** This work was supported by the NSF under a grant of EFMA 1741693 and DMR 1709934. **Author contributions**: Yiling Yu and L.C. conceived the idea. Yiling Yu performed the measurement. Yiling Yu and L.C. designed the experiments, analyzed the data, and wrote the manuscript. Yifei Yu and G.L. helped with the synthesis and transfer of the samples. D.B.G. and A.A.P. performed some of PL and Raman measurements and assisted in writing the manuscript. All the authors were involved in reviewing the manuscript. **Competing interests**: The authors declare that they have no competing interests. **Data and materials availability**: All data needed to evaluate the conclusions in the paper are present in the paper and/or the Supplementary Materials. Additional data related to this paper may be requested from the authors.

Submitted 27 February 2020
Accepted 5 November 2020
Published 18 December 2020
10.1126/sciadv.abb4823

Citation: Y. Yu, Y. Yu, G. Li, A. A. Puretzky, D. B. Geohegan, L. Cao, Giant enhancement of exciton diffusivity in two-dimensional semiconductors. *Sci. Adv.* **6**, eabb4823 (2020).

Giant enhancement of exciton diffusivity in two-dimensional semiconductors

Yiling Yu, Yifei Yu, Guoqing Li, Alexander A. Puretzky, David B. Geohegan and Linyou Cao

Sci Adv **6** (51), eabb4823.
DOI: 10.1126/sciadv.abb4823